The Effects of Numerical Dissipation in Large Eddy Simulations

A. R. BROWN, M. K. MACVEAN, AND P. J. MASON

The Met. Office, Bracknell, Berkshire, United Kingdom

(Manuscript received 19 May 1999, in final form 9 December 1999)

ABSTRACT

Large eddy simulations sometimes use monotone advection schemes. Such schemes are dissipative, and the effective subgrid model then becomes the combined effect of the intended model and of the numerical dissipation. The impacts on simulation reliability are examined for the cases of dry convective and neutral planetary boundary layers. In general it is found that the results in the well-resolved flow interior are insensitive to the details of the advection scheme. However, unsatisfactory results may be obtained if numerical dissipation dominates where the flow becomes less well resolved as the surface is approached.

1. Introduction

A large eddy simulation is based on the concept that the Navier–Stokes equations have been subject to a filter operation. Scales larger than the filter are explicitly represented in the numerical simulation, while a model is used to parametrize the effects of the smaller scales. This parametrization might best be called the ''subfilter model,'' but the term ''subgrid model'' is almost universally used and has been adopted here.

Mason and Brown (1999) (hereafter referred to as MB99) carried out a detailed study of the filtering process in large eddy simulations through examination of the resolved velocity spectra in a series of high-resolution simulations of the dry convective boundary layer in which the basic length scale of the subgrid model (λ_0) and the numerical grid spacing used ($\Delta_{x,y}$) were varied independently. They found that for fixed λ_0, almost identical velocity spectra in the flow interior were obtained from all simulations with $C_s = \lambda_0/\Delta_{x,y} \gtrsim 0.32$, that is, as long as the numerical grid was fine enough, the results obtained were independent of that grid. The steep falloff in the spectra was therefore associated with the filter being applied by the subgrid model and being independent of the numerical mesh, consistent with the ideas of Mason and Callen (1986). Smaller values of C_s were shown to lead to results that diverged from the high-resolution limit and were associated with finite difference errors. Spectral behavior in the near-surface region was also examined. Here obtaining spectra in which a steep falloff (or filtering) occurred at the same scale at all heights was regarded as evidence for successful operation of the subgrid model.

The study of MB99 exclusively used the Piacsek and Williams (1970) form of the nonlinear advection terms, which is centered in space. This numerical procedure (used in conjunction with a leapfrog time-marching scheme) ensures conservation of energy and scalar variance, and so dissipation in the MB99 study was entirely due to the subgrid model. However, particularly when performing large eddy simulations of cloudy boundary layers, it is common practice to use monotone advection schemes (at least on the scalar variables) in order to avoid problems associated with spurious under- and overshoots. When such schemes are used, dissipation from the resolved scales occurs both through the action of the subgrid model *and* through the numerics. The purpose of the present study is to extend the work of MB99 to consider the effects of using schemes that lead to this numerical dissipation. A similar study has recently been performed by Margolin et al. (1999). Both convective and neutral dry boundary layers will be considered here. In each case, a range of simulations will be described in which different fractions of the total dissipation were performed by the subgrid model and by the numerical scheme. Effects on the simulated spectra will be examined and any impacts on the overall reliability of the simulations will be noted. The implications of the results for simulations of cloudy boundary layers which have strong capping inversions are also considered (section 5).

2. Simulations performed

The basic model used in the present study is that described in MB99. The subgrid model is the stability

Corresponding author address: Dr. Andrew Brown, The Met. Office, London Road, Bracknell, Berkshire, RG12 2SZ, United Kingdom.
E-mail: arbrown@meto.gov.uk

TABLE 1. Summary of main runs. Here $\Delta_{x,y}$ is the horizontal grid spacing, λ_0 is the basic length scale of the subgrid model, and $C_s = \lambda_0/\Delta_{x,y}$. Letters ''CD'' indicate that a simulation used centered differences while ''U'' indicates that a simulation used the ULTIMATE QUICKEST advection scheme on all variables.

Run	$\Delta_{x,y}$ (m)	λ_0 (m)	C_s	Advection
Convective simulations				
A14	125.0	14.4	0.12	CD
B14	88.9	14.4	0.16	CD
C14	62.5	14.4	0.23	CD
D14	44.4	14.4	0.32	CD
E14	31.3	14.4	0.46	CD
F14	17.9	14.4	0.81	CD
A14U	125.0	14.4	0.12	U
B14U	88.9	14.4	0.16	U
C14U	62.5	14.4	0.23	U
D14U	44.4	14.4	0.32	U
E14U	31.3	14.4	0.46	U
E25U	31.3	24.9	0.81	U
C07U	62.5	7.2	0.12	U
C04U	62.5	3.6	0.06	U
C02U	62.5	1.8	0.03	U
A00U	125.0	0.0	0.00	U
B00U	88.9	0.0	0.00	U
C00U	62.5	0.0	0.00	U
D00U	44.4	0.0	0.00	U
Neutral simulations				
X08	100.0	8.0	0.08	CD
Y08	53.3	8.0	0.15	CD
Z08	26.7	8.0	0.30	CD
X08U	100.0	8.0	0.08	U
Y08U	53.3	8.0	0.15	U
Z08U	26.7	8.0	0.30	U
X15	100.0	15.0	0.15	CD
X04	100.0	4.0	0.04	CD
X15U	100.0	15.0	0.15	U
X04U	100.0	4.0	0.04	U
X00U	100.0	0.0	0.00	U

dependent version of the Smagorinsky (1963) model that is documented in Brown et al. (1994). However, as well as performing simulations using the standard nondissipative (centered difference) formulation, parallel runs were performed in which the advection scheme (for all variables) was replaced with the ULTIMATE QUICKEST scheme of Leonard et al. (1993). This is a third-order upwind scheme in which a flux limiter eliminates spurious under- or overshoots. It is just one example of a monotone scheme, but others should give qualitatively similar results.

The convective and neutral simulations performed will now be described in turn.

a. Convective simulations

The convective case studied is the same as that used in MB99. Each simulation was initialized with the potential temperature (θ) constant at 300 K from the surface up to $z = 1000$ m, and then increasing linearly at 0.003 K m^{-1} until the domain top at 3000 m. The wind components were set to zero. A small perturbation (± 0.5 K) was applied to the potential temperature at the lowest model level to initiate turbulence, and a heat flux ($\langle w'\theta' \rangle_0$) of 0.06 K m s^{-1} was imposed at the no-slip surface (roughness length set to 0.1 m).

The horizontal domain is a square of side 4000 m. Six different numerical grids have been employed (as in MB99), with $\Delta_{x,y}$ varying between 125 m in grid A (the coarsest) and 17 m in grid F (the finest). In all cases the vertical resolution is at least as good as that in the horizontal. All simulations were run for 10 000 s, with turbulence statistics averaged over the horizontal domain and over the last 4000 s in each case. The resulting boundary layer depth (z_i, defined to be equal to the height of the heat flux minimum) is close to 1000 m in each case, with values of the convective velocity scale, w_*, of around 1.25 m s^{-1}.

A summary of the runs performed can be found in Table 1. The naming convention has been chosen so that the grid resolution (from A to F) and the value of λ_0 used can be immediately ascertained. The letter ''U'' at the end of the name indicates that a simulation used the ULTIMATE QUICKEST advection scheme. Some of the same information is also shown pictorially in Fig. 1a in order to highlight the main comparisons that can be made.

Moving along the horizontal line from A14 to E14 in Fig. 1a shows the effect of varying the grid spacing with fixed subgrid length scale while using nondissipative numerics, exactly as in MB99. The series A14U to E14U exactly parallels A14 to E14, but uses the dissipative ULTIMATE QUICKEST advection scheme. Hence the impact of using such a scheme can be assessed across a range of numerical resolutions: $C_s = 0.12$ in A14 and A14U to $C_s = 0.46$ in E14 and E14U. Point F14 obtained a higher values of C_s by further reducing the grid spacing with fixed subgrid length scale, but in order to show the high C_s limit with monotone advection more cheaply, E25U was performed with the same grid as in E14U but increased λ_0.

When using nondissipative numerics, MB99 showed that the use of small values of C_s ($\lesssim 0.16$) could lead to a buildup of energy close to the grid scale. These are precisely the conditions in which the use of a dissipative numerical scheme might be expected to have most effect. In order to study the behavior of simulations using such a scheme in the small C_s limit, another series of runs was performed (shown dotted in Fig. 1a) in which λ_0 was reduced at fixed grid spacing. The runs C14U, C07U, C04U, and C02U have C_s values of 0.23, 0.12, 0.06, and 0.03, respectively, and C00U is the extreme case in which $\lambda_0 = 0$, that is, the subgrid model is entirely switched off and all dissipation is performed by the numerical scheme. Finally, comparison of A00U, B00U, C00U, and D00U shows the resolution dependence of the results in this ''no subgrid model'' limit.

b. Neutral simulations

The neutral simulations performed were of flows driven by an imposed pressure gradient which, together with

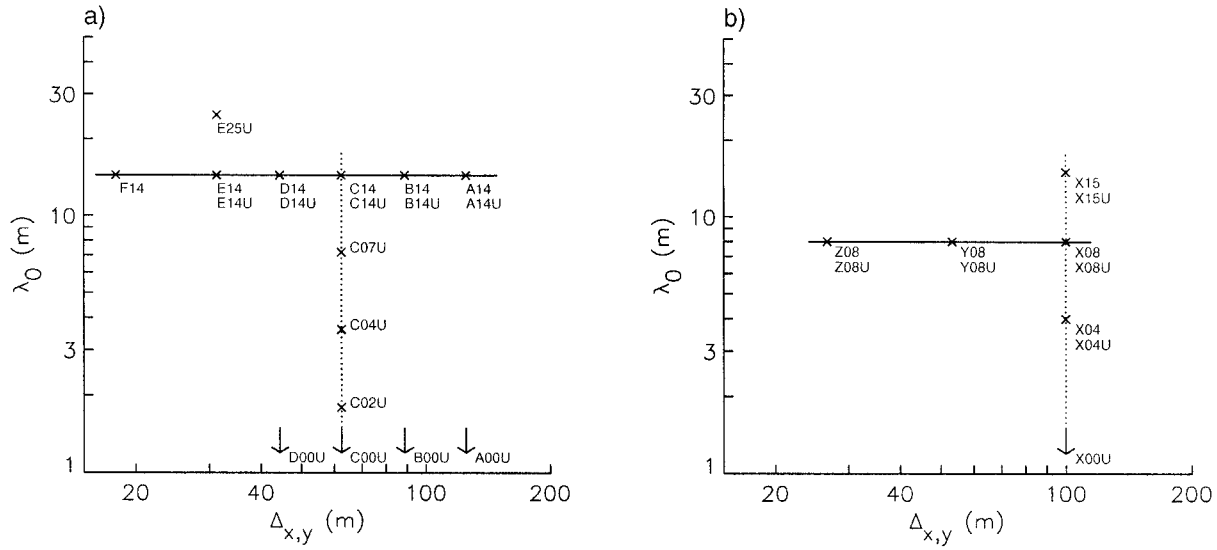

FIG. 1. Horizontal grid spacing ($\Delta_{x,y}$) and subgrid length scale (λ_0) of the main simulations. (a) Convective simulations, (b) neutral simulations. ''U'' in a simulation name indicates that that simulation used the monotone ''ULTIMATE'' advection scheme of Leonard et al. (1993).

the value of the Coriolis parameter appropriate to 45°N, gave a geostrophic wind (G) of 10 m s^{-1}. The surface roughness length was set to 0.1 m. The initial wind profiles were geostrophic and small perturbations were applied to the vertical velocity field in order to initiate turbulence. The simulations were run for 100 000 s, with turbulence statistics averaged over the last 30 000 s in each case.

In all cases the domain measured 4800 m (in the geostrophic wind direction) by 3200 m (in the cross wind direction) by 5000 m (in the vertical). Given an expected Ekman layer depth of around 1500 m, this domain size is consistent with that recommended by Mason and Thomson (1987). Three different numerical grids have been used, X, Y, and Z, with a horizontal spacings of 100, 53, and 26 m, respectively. The vertical resolution is at least as good as the horizontal and is finer close to the surface where the grids are refined. Once again simulations have been performed with and without the monotone advection scheme, and with various values of λ_0, as shown in Table 1 and Fig. 1b.

3. Results from convective simulations

Figure 2 shows normalized one-dimensional vertical velocity spectra at $z/z_i = 0.7$ from some of the convective simulations. The spectra have been taken in the x direction and averaged over the y direction and over time. The results from simulations A14, B14, C14, D14, and E14 in Fig. 2 are those that were presented and discussed in MB99. Those from E14 ($C_s = 0.46$) and D14 ($C_s = 0.32$) are very similar to each other, and to those from F14 ($C_s = 0.81$, not shown). This is consistent with the filter being determined by the subgrid model and the results being independent of the grid as long as C_s is large enough. As C_s is reduced finite difference errors make the results less satisfactory with a buildup of energy close to the grid scale and, in A14 ($C_s = 0.12$), a statistically significant loss of variance at larger scales.

The effects of using a monotone advection scheme are now considered. In the well-resolved limit (large C_s) there is little energy close to the grid scale even in the absence of a monotone advection scheme, and so relatively little dissipation occurs through the numerical scheme and the results are similar to those obtained using centered differences. This is illustrated in Figs. 2a and 2b, which show the very similar vertical velocity spectra obtained in E14 and E14U. As C_s is reduced (by increasing the grid spacing at fixed λ_0) the differences between the monotone advection and centered difference solutions become more marked. Numerical dissipation by the monotone advection scheme becomes progressively more important and prevents any buildup of energy close to the grid scale (so that the effective filter scale becomes proportional to the grid scale). In some respects this is clearly beneficial, and A14U is a more satisfactory solution than A14, not showing the same loss of variance at larger scales. However, it will be shown later in this paper that relying on dissipation by a monotone advection scheme to compensate for the use of too small a value of C_s may not be successful in all cases. Figure 2c compares spectra from simulations with a fixed grid and varying λ_0. As λ_0 is reduced the results converge toward the limiting case of C00U in which the subgrid model is turned off. Cases C02U and C04U give solutions close to that of C00U, while C07U and C14U show a steeper spectral falloff as the subgrid model takes increasing significance.

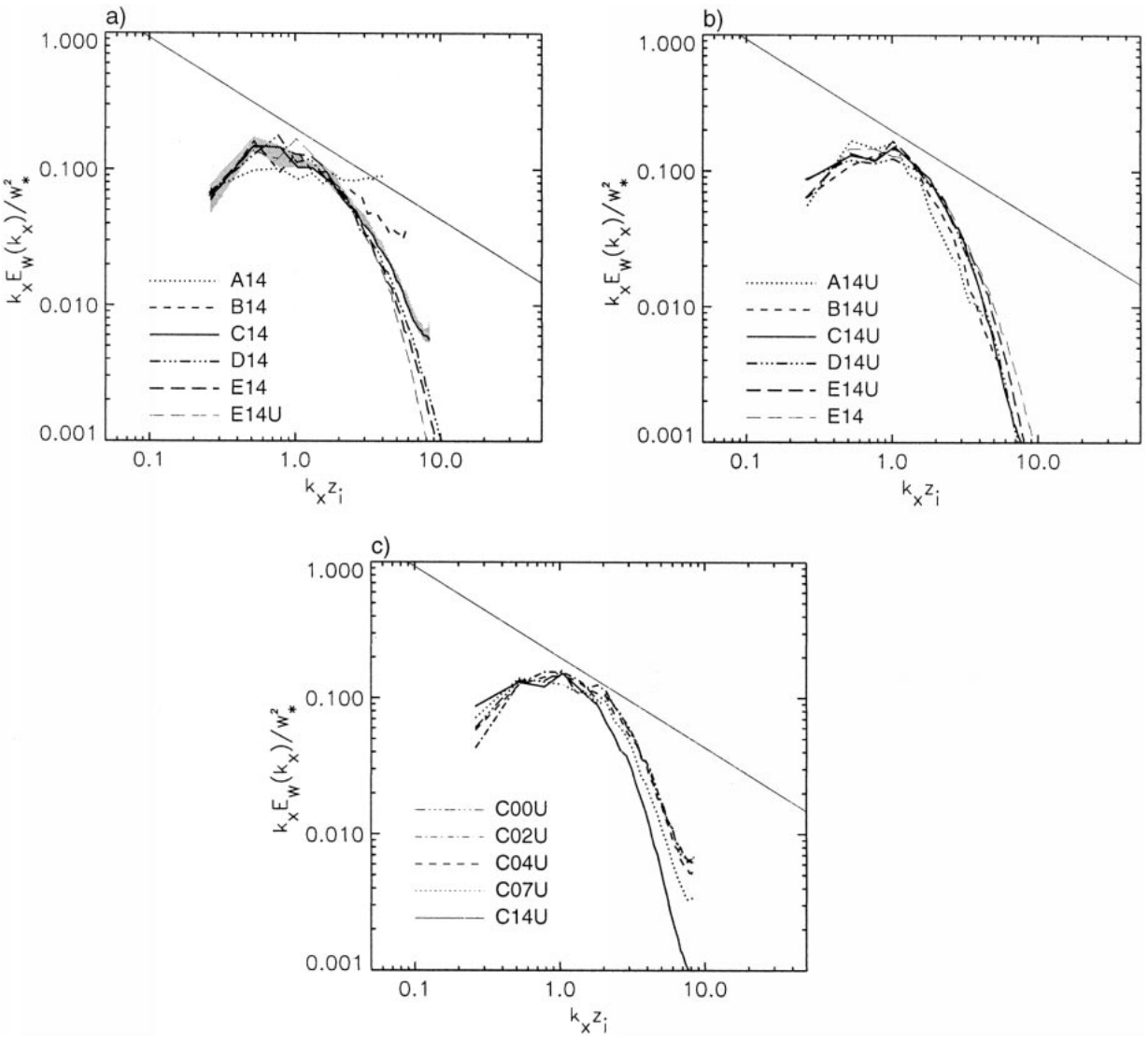

FIG. 2. Normalized one-dimensional w spectra at $z/z_i = 0.7$. The spectra have been taken in the x direction, and k_x is the wavenumber (=1/wavelength). The straight line indicates the $-\frac{2}{3}$ slope that is expected in an inertial subrange. (a) Simulations A14, B14, C14, D14, E14, and E14U; (b) simulations A14U, B14U, C14U, D14U, E14U, and E14; (c) simulations C00U, C02U, C04U, C07U, and C14U. The shaded region in (a) shows the range of results obtained in four successive averaging periods of 4000 s from simulation C14 and is shown to give an idea of the statistical reliability of the results.

Figure 3 shows the total kinetic energy budgets (normalized by w_*^3/z_i where w_* is the convective velocity scale) for simulations B14 and B14U. All terms have been calculated consistently with the model's *actual* finite difference formulation so that exact, consistent budgets can be calculated both for the centered difference and for the monotone advection simulations. Term A is that resulting from the nonlinear advection term in the momentum equations. For B14, with its nondissipative numerics, this is exactly the turbulent transport term that has a vertically averaged value of zero. Here P is the pressure transport term and B and ϵ_{SG} are the buoyancy production and subgrid dissipation terms, respectively. The profiles of B and P from B14U are similar to those from B14, although with some minor differences close to the surface and to the inversion. However, the magnitude of ϵ_{SG} is reduced relative to that in B14 as a significant fraction of the total dissipation is now performed through the monotone advection scheme (vertically averaged value of A now negative). If a turbulent transport term is diagnosed consistent with a centered difference formulation, then the difference between A and this estimate of the transport provides an approximate profile of the numerical dissipation. The crosses in Fig. 3b show the sum of this estimated numerical dissipation and the diagnosed subgrid dissipation for simulation B14U, and this total dissipation profile can be seen to be broadly similar to that of ϵ_{SG} from B14.

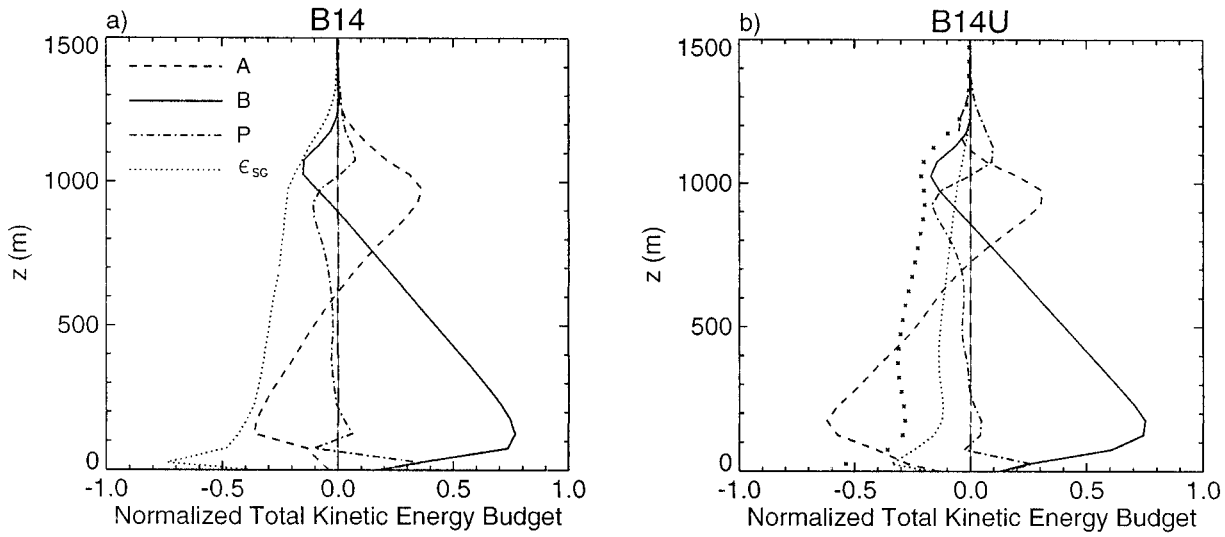

FIG. 3. Normalized total kinetic budgets. Here, A is the term in the budget resulting from the nonlinear term in the momentum equation, B is the buoyancy production, P is the pressure transport term, and ϵ_{SG} is the dissipation due to the subgrid model. (a) Simulation B14, (b) simulation B14U. The crosses in (b) show an estimated profile of total dissipation in B14U, obtained as described in the text.

The profiles of buoyancy production and pressure transport from the other simulations are similar to those from B14 and B14U and so are not shown here. Figure 4a confirms that the vertically averaged buoyancy production [$B^A = (1/z_i)\int_0^{z_i} B\,dz$] is almost constant across the centered difference simulations with $\lambda_0 = 14.4$ m (A14 to F14), and that it is little changed in the simulations using the monotone advection scheme (A14U to E14U). This plot also quantifies the partition between dissipation due to the subgrid model and dissipation due to the model numerics. For the centered difference simulations the average of term A is zero and there is no numerical dissipation, so the averaged buoyancy production is entirely balanced by the averaged subgrid dissipation (ϵ^A_{SG}). For the monotone advection simulations the numerical dissipation ($\epsilon^A_{NUM} \equiv A^A$) increases while the subgrid dissipation decreases as the grid spacing becomes coarser (with the sum of the two balancing the near-constant buoyancy production). The fraction of the total dissipation (ϵ^A_{TOT}) performed by the numerical

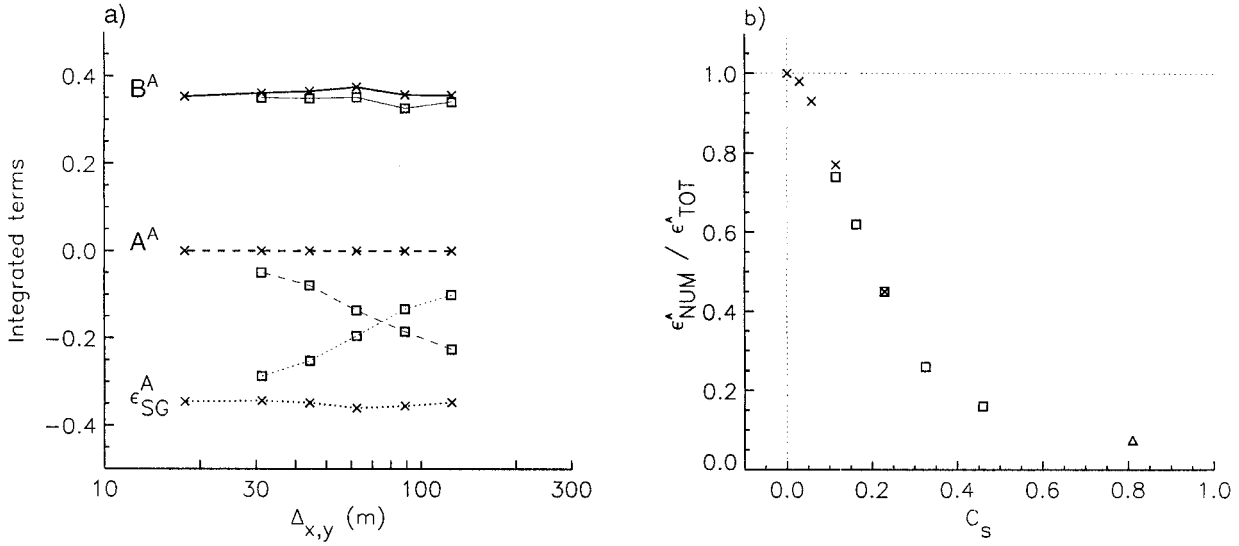

FIG. 4. (a) Normalized vertically averaged terms in the total kinetic energy budgets from simulations with $\lambda_0 = 14.4$ m. Solid lines: B^A, averaged buoyancy production; dotted lines: ϵ^A_{SG}, averaged subgrid dissipation; dashed lines: A^A, averaged effect of advective terms. Crosses and heavy lines: simulations using centered differences; squares and light lines: simulations using monotone advection. (b) Ratio of vertically averaged numerical dissipation to vertically averaged total dissipation for all convective simulations using the monotone advection scheme. Crosses: simulations using grid C; squares: simulations using $\lambda_0 = 14$ m; Triangle: simulation E25U.

scheme is shown as a function of C_s in Fig. 4b, with results plotted for all of the convective runs using monotone advection. The form is as expected, with $\epsilon^A_{\rm NUM}/\epsilon^A_{\rm TOT} = 1$ at $C_s = 0$ and asymptoting to zero as C_s becomes large. The commonly used value of $C_s = 0.23$ gives $\epsilon^A_{\rm NUM}/\epsilon^A_{\rm TOT} \simeq 0.45$, although it is stressed that this value is not expected to be universal. In fact, the exact form of the curve of $\epsilon^A_{\rm NUM}/\epsilon^A_{\rm TOT}$ against C_s will be dependent on the details of the monotone advection scheme used, and it will also be dependent on the flow type and on the value of λ_0 if the simulation does not resolve well into the inertial subrange.

The preceding paragraphs have highlighted the effects on the simulated spectra and energy budgets of using different resolutions and values of subgrid length scale, and of changing between nondissipative and dissipative advection schemes. However, it should be emphasized that many of the turbulence statistics (e.g., variance and flux profiles) are robust across these changes. Only simulation A14 (nondissipative numerics and a low value of C_s leading to a buildup of energy close to the grid scale) shows velocity variance profiles that are clearly unsatisfactory. In the interior of the convective boundary layer case chosen in this series of simulations, the spectral peak is reasonably well resolved and it appears that the most critical requirement is simply that there should be enough dissipation (be it through the subgrid model or the numerical scheme) to prevent a buildup of energy close to the grid scale. These findings are consistent with those of Margolin et al. (1999). However, close to a boundary (surface or inversion) the turbulence will inevitably be less well resolved, and examination of statistics in these regions may provide a more discriminating test of the performance of a model. As an example, the mean potential temperature profiles obtained in a number of the simulations are now examined.

Figure 5a shows the potential temperature profiles from simulations A14, B14, C14, D14, E14, and F14 (adjusted to have the same value at 100 m in order to highlight any differences in the surface layer). In spite of the varying resolutions (both horizontal and vertical), it is encouraging that all of the simulations can be seen to follow approximately the same curve. The slight differences that do occur close to the surface are probably associated with the presence of finite difference errors in the less well resolved simulations (A14, B14, and C14). The use of a monotone advection scheme prevents buildup of energy near the grid scale, and the mean potential temperature profiles from A14U, B14U, C14U, D14U, and E14U (Fig. 5b) are all virtually identical to those from the better-resolved simulations using centered differences (D14, E14, and F14). Hence it appears that, as in the flow interior, dissipation from a monotone advection scheme may in some respects compensate for the use of a low value of C_s ($=0.12$ in A14 and A14U). However, less satisfactory effects are seen when C_s is reduced still further (by reducing λ_0). Figure 5c shows potential temperature profiles from C14U, C07U, C04U, C02U, and C00U (C_s values of 0.23, 0.12, 0.06, 0.03, and 0.00, respectively). As C_s is reduced there is a significant warming at the lowest model level, reaching around 0.5 K in the limiting case of C00U in which the subgrid model has been turned off. At the same time there is a slight cooling higher up in the simulated surface layers. That these profiles are unreliable can be seen in Fig. 5d, which shows the solutions obtained in A00U, B00U, C00U, and D00U. These simulations differ only in their resolution (all having the subgrid model switched off), and yet there is no sign of convergence of the solutions, with the height at which the large potential temperature gradient occurs in each case clearly being controlled by the height of the lowest model grid level.

The reason for the unsatisfactory sensitivity to resolution of the profiles obtained when using a monotone advection scheme without a subgrid model is almost certainly that there can be no subgrid flux and so the buoyancy flux has to be 100% resolved at the first model level. The simulation can only achieve the required resolved flux by having more resolved variance at low levels, which in turn can only be achieved by having a more unstable mean temperature profile. To illustrate the differences in low-level resolved variance, Fig. 6 shows one-dimensional vertical velocity spectra at 20, 40, 80, 160, and 320 m from simulations D14 and D00U (averaged across the domain but not over time). Those from D14 (and from D14U, not shown, which are almost identical) show, at all levels, a sharp falloff in spectral energy at small scales. The results from D00U remain satisfactory in as much as there is no buildup of energy at the grid scale, but the increase in resolved variance close to the surface is clear. As C_s is increased above zero, the fraction of the total flux that has to be resolved at the first model level becomes smaller (e.g., $\cong 0.25$ at $z = 20$ m in D14, which has $C_s = 0.32$), reducing the need for a spuriously large unstable temperature gradient and leading to the largely resolution independent results shown in Figs. 5a and 5b.

4. Results from neutral simulations

The results from the neutral simulations illustrate many of the same points found in the analysis of the convective simulations. However, they are presented as well in order to show more dramatically the sensitivity to subgrid model and numerical scheme that can be encountered in regions where the turbulence is not well resolved. The extra sensitivity in this case arises because the shear production of turbulence itself depends strongly on the simulated mean and turbulent fields (whereas in the convective case, the buoyancy production was effectively imposed through the choice of surface heat flux). The convective case would be expected to show an increased sensitivity if the surface temperature (rather than the heat flux) were fixed in value.

The comparison of the results of the neutral simulations using a fixed subgrid length scale of 8 m is considered first. Figure 7 shows instantaneous vertical

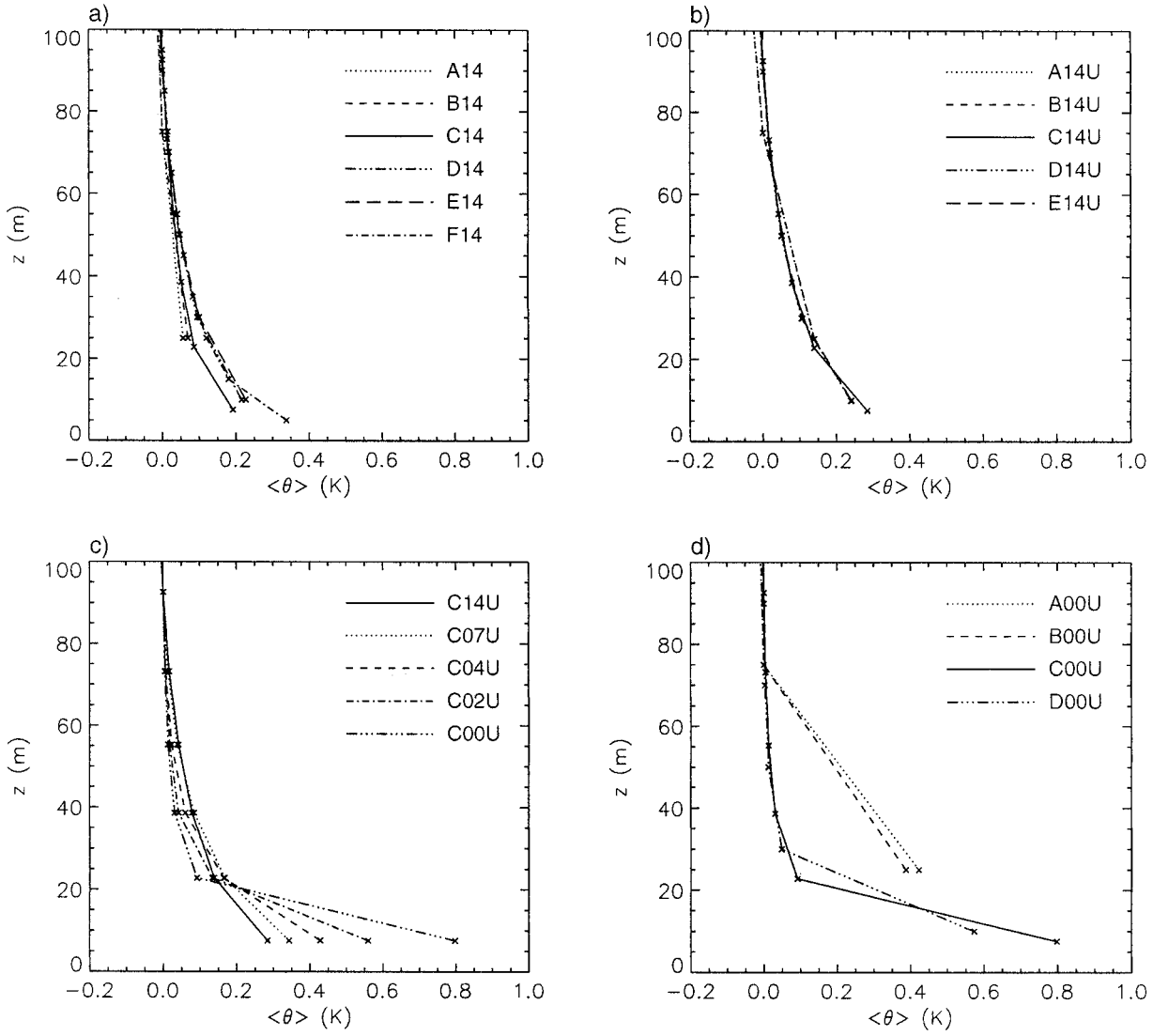

FIG. 5. Near-surface mean potential temperature profiles (adjusted so that all have value zero at 100 m). (a) Simulations A14, B14, C14, D14, E14, and F14; (b) simulations A14U, B14U, C14U, D14U, and E14U; (c) simulations C14U, C07U, C04U, C02U, and C00U; (d) simulations A00U, B00U, C00U, and D00U.

velocity spectra at five different levels from these runs (normalized using the friction velocity, u_*). The centered difference simulation Z08 has the finest of the three meshes ($\Delta_{x,y} = 26$ m; $C_s = 0.3$), and the spectra show well-defined peaks that move, as expected, to larger scale as the distance from the surface increases. A sharp spectral falloff (at $k_x z_i \cong 20$) due to the subgrid model is seen at all levels. The normalized mean velocity profile from this simulation is shown in Fig. 8a. It deviates from the logarithmic profile (indicated by crosses), in the semiresolved region at around 100 m where it shows excessive shear, leading to a predicted geostrophic drag coefficient, $C_G = u_*^2/G^2 = 1.76 \times 10^{-3}$, which is low compared to observed values (e.g., Grant 1986) of around 2×10^{-3}. This failing of the Smagorinsky subgrid model is well known, and more advanced models have been developed to alleviate it [e.g., the backscatter model of Mason and Thomson (1992) and the two-part viscosity model of Sullivan et al. (1994)]. However, the results are adequate for present purposes, which seek only to demonstrate that there exists a potentially large sensitivity of large eddy simulation results in the surface layer to the numerical methods used.

The spectra from simulation Y08 (Fig. 7) ($\Delta_{x,y} = 53$ m; $C_s = 0.15$) are very similar to those from Z08 over the range of scales captured by both simulations, but the buildup of energy close to the grid scale in X08 indicates that its numerical resolution ($\Delta_{x,y} = 100$ m; $C_s = 0.08$) is inadequate. The resulting velocity profiles (Fig. 8a) are similar, but not identical, to those from Z08. The fact that they have moved toward a more

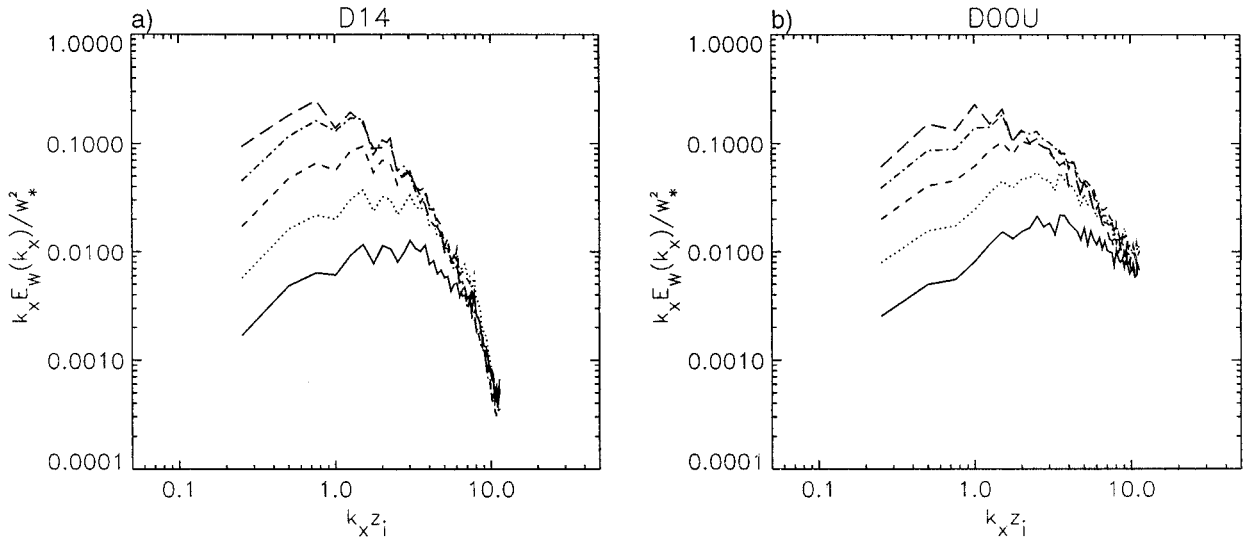

FIG. 6. Normalized one-dimensional w spectra at 20 (solid), 40, 80, 160, and 320 m (long dashes). (a) D14, (b) D00U.

realistic logarithmic profile should not be regarded as evidence of success, as the changes from the results of Z08 arise solely because of a less faithful representation of the continuous solution due to the use of a coarser numerical mesh. Note that these results are entirely analogous to the centered difference convective results; use of too small values of C_s led to buildup of energy close to the grid scale and small departures of the mean profiles in the surface layer from those obtained in the better resolved runs (Fig. 5a).

The effects of employing the monotone advection scheme are now examined. Figure 7 shows that its use has little effect on the spectra at $C_s = 0.3$ (Z08U compared to Z08), but that its impact increases as C_s decreases; the spectra from Y08U and X08U show an increasing loss of variance, with the sharp spectral falloff moving to larger scale. Interestingly, only 15% of the total kinetic energy dissipation is performed by the numerical scheme in X08U, compared with around 80% obtained in a convective simulation at the same value of C_s (Fig. 4b). This difference probably arises because the neutral simulations are not well resolved close to the surface where most of the dissipation occurs. This means that a large proportion (77% for X15; 70% for Y08) of the total dissipation due to the subgrid model is directly of the kinetic energy of the mean flow, rather than of turbulent kinetic energy. As the range of scales represented is increased (at fixed C_s), a greater proportion of the total dissipation is from the turbulent kinetic energy and, in runs using the monotone advection scheme, this leads to an increase in the relative importance of numerical dissipation (10% of the total dissipation in X15; 14% in Y08).

Although the fraction of the total dissipation performed by the numerical scheme in Z08U, Y08U, and X08U is not large, significant differences are seen between the simulated velocity profiles (Fig. 8a). Simulation Z08U (which has the finest numerical resolution of the three) has a profile similar to that obtained in the three runs using centered differences. However, as C_s is reduced, the differences from the results obtained using centered differences increase, with the simulated shear becoming progressively more excessive. The explanation for these changes is that, if the mean velocity profiles were fixed, then the effect of introducing the monotone advection scheme that removes small-scale energy would be to reduce the resolved momentum flux. However, the new total flux would not be consistent with the mean velocity profile (from momentum budget considerations), and so the simulation using the monotone advection scheme has to somehow increase the resolved and/or subgrid fluxes. Both of these can be achieved by increasing the mean shear, leading to the results shown in Fig. 8a. The same effect is seen in the series of simulations that use grid X (Fig. 8b): the simulations using monotone advection systematically show greater shear than corresponding runs using centered differences, and the differences between the results of the two schemes increase as C_s decreases. Once again these results are qualitatively the same as those of the convective simulations, the use of low C_s and monotone advection leading to increased mean gradients in the surface layer (Fig. 5c). The limiting case of switching the subgrid model off altogether (X00U) leads to completely unrealistic results in the neutral case, with no sign of a logarithmic profile (Fig. 8b) and a geostrophic drag coefficient an order of magnitude smaller than the observed value.

5. Effects in an inversion region

The present results have shown a lack of sensitivity to the details of the numerical methods and subgrid model in the well-resolved interior of the flow. However,

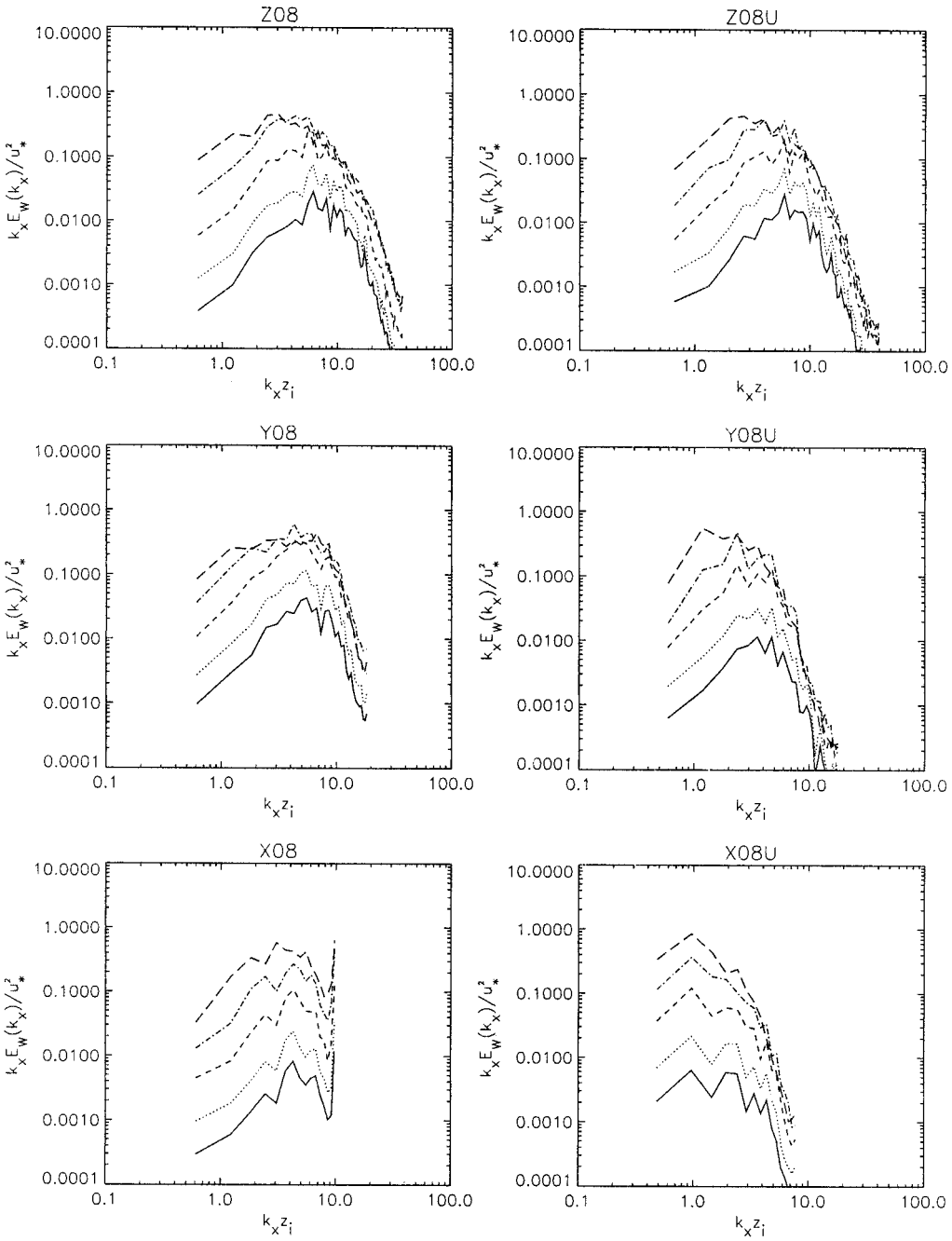

FIG. 7. Normalized one-dimensional *w* spectra at 20 (solid), 40, 80, 160, and 320 m (long dashes) from the neutral simulations with $\lambda_0 = 8$ m.

as the surface is approached the eddy resolution becomes marginal, the fluxes (in a simulation with an explicit subgrid model) become predominantly subgrid, and the results inevitably become sensitive to the details of the subgrid model and advection scheme. Relying entirely on numerical dissipation from the advection scheme (with no explicit subgrid model) has been shown to lead to a lack of convergence of the results in this region as the resolution is increased.

The situation close to the capping inversion at the top of the boundary layer is not entirely analogous to that close to the surface due to the absence of a rigid surface and zero vertical velocity boundary condition. This means that the modeled entrainment fluxes at the boundary layer top tend to be on large scales and remain well resolved (e.g., Bretherton et al. 1999). However, the characteristic turbulence length scale will reduce close to the inversion and so the resolution of important small-

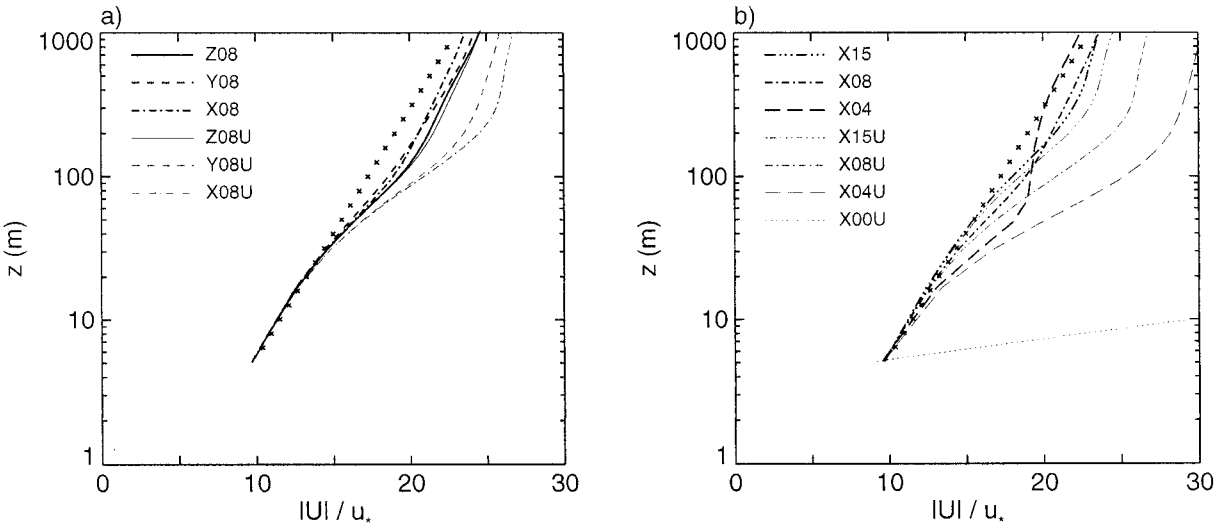

FIG. 8. Normalized velocity profiles from the neutral simulations. The crosses indicate a logarithmic profile.

er-scale motions may again become marginal. Therefore the results in this region might also be expected to become more sensitive to the choice of advection scheme and subgrid model. There is some evidence that this is the case in the convective boundary layer simulations. For example, consider A_1, the ratio of the maximum magnitude of the downward total heat flux at the inversion to the magnitude of the surface heat flux. It has values of 0.14 in D14, 0.16 in D14U, and 0.18 in D00U; that is, there is a tendency toward rather larger entrainment fluxes as the numerical dissipation becomes relatively more important (although the changes are not large enough to impact significantly on the integrated buoyancy fluxes discussed in section 3).

Simulations of cloudy boundary layers might be expected to present greater difficulties for the large eddy technique, as radiative cooling at cloud top often leads to the presence of much stronger capping inversions than found in the dry case. As a simpler example of a case with a stronger inversion, boundary layers capped with radiatively active smoke or dust clouds have been extensively modelled, for example, the model intercomparison study of Bretherton et al. (1999). Here four simulations have been performed of the standard case from that study, using a horizontal resolution of 50 m and a vertical spacing of 10 m in the inversion region. Simulations D12CC, D12CU, and D12UU all used a basic subgrid length scale of 11.5 m ($C_s = 0.23$) and used, respectively, centered differences on both scalars and momentum, ULTIMATE on scalars and centered differences on momentum, and ULTIMATE on both scalars and momentum. D00UU used ULTIMATE on scalars and momentum and had the explicit subgrid model turned off. Time series of inversion height (defined as in Bretherton et al.) from these four simulations are shown in Fig. 9. There is clearly some spread in the modeled entrainment rates, although it is rather smaller than that found between different models in the intercomparison study. Furthermore, the results from the fully centered simulation (D12CC) should possibly be disregarded in this comparison, as the overshoots associated with the use of centered differences are quite significant at $C_s = 0.23$, leading to negative smoke concentrations that interact strongly with the radiation scheme. Investigation of the reasons for the remaining spread (the sense of which is opposite to that found in the convective boundary layer runs, with the use of ULTIMATE here leading to smaller entrainment rates) is beyond the scope of the present paper. The reader is referred to the study of Stevens et al. (1999), which discusses in detail the behavior of large eddy simulations in the inversion region and sensitivity to subgrid model. However, as noted by Stevens et al., very much

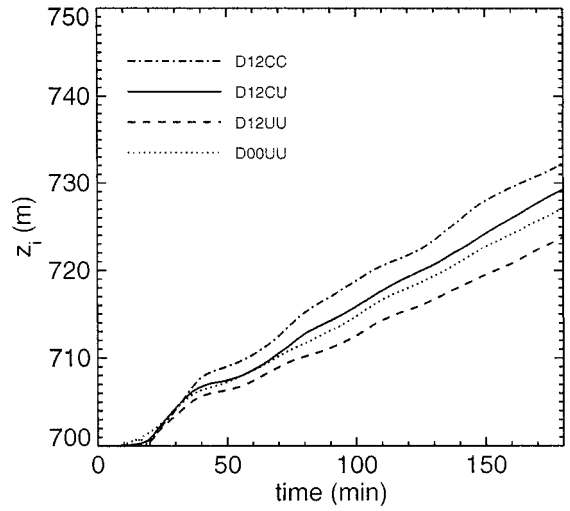

FIG. 9. Time series of inversion height for four simulations of the Bretherton et al. (1999) smoke cloud case (see text for details).

higher resolution simulations are required in order to assess the convergence properties of the solutions obtained with different subgrid models and advection schemes. Until such time as computational resources permit such simulations to be performed, we can do no more than note that, at current resolutions, the simulated entrainment rates do show some sensitivity to the choice of advection scheme and subgrid model.

6. Conclusions

This study considers the use of an explicit subgrid model in combination with a monotone advection scheme. With a fixed length scale in the subgrid model, a previous study (MB99), which used nondissipative numerics, found that with a sufficiently fine numerical mesh the results converged and became independent of the numerical mesh. For a convective atmospheric boundary layer this convergence became evident for $C_s \gtrsim 0.3$. Here, with the additional consideration of a monotone advection scheme, the MB99 result remains unchanged, and for $C_s \gtrsim 0.3$ the choice of advection scheme has no significant influence on the results.

For smaller values of C_s the use of a monotone advection scheme has an impact and the subgrid model is now the combined effect of the intended scheme and of the numerical dissipation. It is now hard to explicitly separate the effects, although the present study shows that diagnostics consistent with energy conserving numerical forms can provide a posteriori estimates.

If the interior regions of the flow are considered separately, it is clear that when the flow is modeled well into the inertial subrange, the results are insensitive to the details of the subgrid model and to the choice of advection scheme (as long as there is enough dissipation to prevent buildup of energy at small scales). The results obtained using the monotone advection scheme alone (with no subgrid model) seem quite satisfactory and are in some respects better than those obtained using nondissipative numerics with values of $C_s \lesssim 0.15$. It can therefore be argued that, for such regions, the use of the monotone advection scheme alone is both effective and computationally efficient. These findings are consistent with those of Margolin et al. (1999).

However, all boundary layer flows will have critical wall regions where the turbulence is not well resolved and the simulation must match to an explicitly determined near-wall behavior. In these regions the length scale in the subgrid model is linked to distance from the wall. When a monotone advection scheme is used in conjunction with small values of C_s, the simulated mean gradients have to increase in order to maintain the fluxes required for equilibrium, and the results do not converge with increasing resolution. In the case of a convective boundary layer with the surface heat flux specified, this leads to errors in surface temperature and the influence is mainly in near-surface statistics. When constant value boundary conditions are specified as in the case of a neutral static-stability planetary boundary layer with a no-slip condition for velocity, the mean gradient errors lead to flux errors that can impact on the entire flow. Results for entrainment at the top of the boundary layer have also been shown to show some sensitivity to the choice of advection scheme, although in this case it has not proved possible to demonstrate whether relying on numerical dissipation leads to less satisfactory convergence properties.

Note that all of the monotone advection simulations showed apparently satisfactory spectral rolloff at small scales. MB99 argued that this behavior is a necessary condition for successful operation of a subgrid model. However, the fact some of the simulations that met this requirement for a steep spectral falloff showed excessive mean gradients in the surface layer indicates that, while necessary, it is not a sufficient condition.

To summarize, large eddy simulation results appear to be encouragingly insensitive to the choice of advection scheme, as long as the simulation is well resolved, either numerically (high C_s) or in the sense of the filter being well into the inertial subrange. Close to the surface, the latter criterion cannot be satisfied, and this region will always be a source of some difficulty. If the dissipation remains primarily through the subgrid model (high C_s and/or nondissipative numerics) then reasonable results may still be obtained, as some progress has been made in linking the subgrid model, at least crudely, to the expected near-surface behavior (e.g., through making modifications to the length scale and through using stability functions consistent with surface-layer similarity). It is suggested that the degradation found in the results when dissipation by the numerical scheme dominates in this region occurs because there is no corresponding linkage of the scheme to the correct near-wall behavior in this case.

REFERENCES

Bretherton, C. S., and Coauthors, 1999: An intercomparison of radiatively driven entrainment and turbulence in a smoke cloud, as simulated by different numerical models. *Quart. J. Roy. Meteor. Soc.*, **125,** 391–423.

Brown, A. R., S. H. Derbyshire, and P. J. Mason, 1994: Large-eddy simulation of stable atmospheric boundary layers with a revised stochastic subgrid model. *Quart. J. Roy. Meteor. Soc.*, **120,** 1485–1512.

Grant, A. L. M., 1986: Observations of boundary layer structure made during the KONTUR experiment. *Quart. J. Roy. Meteor. Soc.*, **112,** 825–841.

Leonard, B. P., M. K. MacVean, and A. P. Lock, 1993: Positivity-preserving numerical schemes for multidimensional advection. NASA Tech. Memo. 106055 (ICOMP-93-05), 62 pp.

Margolin, L. G., P. K. Smolarkiewicz, and Z. Sorbjan, 1999: Large-eddy simulations of convective boundary layers using nonoscillatory differencing. *Physica D.*, **133,** 390–397.

Mason, P. J., and N. S. Callen, 1986: On the magnitude of the subgrid-scale eddy coefficient in large-eddy simulations of turbulent channel flow. *J. Fluid Mech.*, **162,** 439–462.

——, and D. J. Thomson, 1987: Large eddy simulation of the neutral-static-stability planetary boundary layer. *Quart. J. Roy. Meteor. Soc.,* **113** 413–443.
——, and ——, 1992: Stochastic backscatter in large-eddy simulations of boundary layers. *J. Fluid Mech.,* **242,** 51–78.
——, and A. R. Brown, 1999: On subgrid models and filter operations in large-eddy simulations. *J. Atmos. Sci.,* **56,** 2101–2114.
Piacsek, S. A., and G. P. Williams, 1970: Conservation properties of convection difference schemes. *J. Comput. Phys.,* **6,** 392–405.
Smagorinsky, J., 1963: General circulation experiments with the primitive equations: 1. The basic experiment. *Mon. Wea. Rev.,* **91,** 99–164.
Stevens, B., C.-H. Moeng, and P. P. Sullivan, 1999: Large-eddy simulations of radiatively driven convection: Sensitivities to the representation of small scales. *J. Atmos. Sci.,* **56,** 3963–3984.
Sullivan, P. P., J. C. McWilliams, and C.-H. Moeng, 1994: A subgrid-scale model for large-eddy simulation of planetary boundary layer flows. *Bound.-Layer Meteor.,* **71,** 247–276.